Optically detected spin-mechanical resonance in silicon carbide membranes

Poshakinskiy, A. V.; Astakhov, G.;

Originally published:

September 2019

Physical Review B 100(2019), 094104

DOI: https://doi.org/10.1103/PhysRevB.100.094104

Optically detected spin-mechanical resonance in silicon carbide membranes

A. V. Poshakinskiy[1] and G. V. Astakhov[2,1]
[1] *Ioffe Institute, 194021 St. Petersburg, Russia*
[2] *Helmholtz-Zentrum Dresden-Rossendorf, Institute of Ion Beam Physics and Materials Research, 01328 Dresden, Germany*
(Dated: January 29, 2019)

Hybrid spin-mechanical systems are a promising platform for future quantum technologies. Usually they require application of additional microwave fields to project integer spin to a readable state. We develop a theory of optically detected spin-mechanical resonance associated with half-integer spin defects in silicon carbide (SiC) membranes. It occurs when a spin resonance frequency matches a resonance frequency of a mechanical mode, resulting in a shortening of the spin relaxation time through enhanced spin-phonon coupling. The effect can be detected as an abrupt reduction of the photoluminescence intensity under optical pumping without application of microwave fields. We propose all-optical protocols based on such spin-mechanical resonance to detect external magnetic fields and mass with ultra-high sensitivity. We also discuss room-temperature nonlinear effects under strong optical pumping, including spin-mediated cooling and heating of mechanical modes. Our approach suggests a new concept for quantum sensing using spin-optomechanics.

I. INTRODUCTION

Cavity optomechanics is an emerging research field exploring the interaction between electromagnetic radiation and mechanical resonators [1]. The motivation for the research originates from exciting fundamental physics as well as various technological applications, including high-resolution accelerometers [2] and quantum transducers [3]. The interaction between light and nanomechanical modes can also be mediated by electron spin qubits [4–6]. Indeed, such a hybrid spin-mechanical quantum system have been realized using the NV center in diamond [7–14]. Silicon carbide (SiC) is a natural platform for spin optomechanics, as it is used as a material for ultra-sensitive nano-electromechanical systems (NEMS) [15–17] and simultaneously hosts highly-coherent spin centers, such as silicon vacancies (V_{Si}) [18] and divacancies (VV) [19]. Recently, mechanical tuning [20] and acoustic coherent control [21] of the VV spin-1 centers in SiC has been experimentally demonstrated.

In this work, we consider theoretically the interaction between spin qudits ($S = 3/2$) [22] and vibrational modes of a SiC membrane. Using the temperature dependence of the spin-lattice relaxation time, we extract the deformation potential constant and discuss realistic applications of such a hybrid quantum system. Particularly, we proposes an all-optical protocol for the DC magnetometry when the sensitivity is defined by the mechanical Q-factor of the membrane. We also discuss all-optical cooling efficiency of vibrational modes in a SiC membrane at room temperature, when they interact with a dense V_{Si} spin ensemble, and suggest an all-optical protocol for chemisorption measurements based on the mass-dependent shifts of the mechanical modes. Finally we discuss how the static strain of the membrane can be mapped via the shift of the zero-splitting and propose to use it for force or acceleration measurements.

II. SPIN-PHONON INTERACTION

While our theoretical approach is general, we use the experimental parameters for the so-called V_{Si}(V2) spin qudit in 4H-SiC [23] to link it to practical applications. It has spin $S = 3/2$ in the ground state [24], which is split in two spin sublevels $m_S = \pm 3/2$ and $m_S = \pm 1/2$ with the zero-field splitting $2D = 70\,\mathrm{MHz}$ [25]. First, we discuss how such spin centers interact with lattice vibrations.

Vibrations create local deformations that affects the spin states associated with point defects in the crystal. The Hamiltonian, describing this spin-phonon interaction, can be constructed using the group representation theory [26, 27]. For the sake of simplicity, we use the spherical approximation, where the interaction Hamiltonian reads

$$H_{\mathrm{def}} = \Xi u_{\alpha\beta} S_\alpha S_\beta \,. \tag{1}$$

Here, Ξ is the deformation potential constant, $u_{\alpha\beta}$ is the deformation tensor, $\boldsymbol{S} = (S_x, S_y, S_z)$ is the vector of spin-3/2 operators. We note, that Hamiltonian (1) should be even in spin operators due to the time-inversion symmetry. In case of static deformation, Eq. (1) describes modification of the zero-field splitting and spin level mixing, as discussed in Sec. IV D.

When $u_{\alpha\beta}$ is regarded as a deformation induced by phonons passing by the spin center, Eq. (1) can be used to calculate the rate of the direct transitions $W^{(\mathrm{direct})}_{m'_S,m_S}$ between the sublevels with the spin projection on the c-axis m_S and m'_S [28]. We get

$$W^{(\mathrm{direct})}_{\pm 3/2,\pm 1/2} = \frac{\Xi^2 |E_{\pm 3/2} - E_{\pm 1/2}|^2}{2\pi\hbar^4 \rho \bar{v}^5} k_B T \,, \tag{2}$$

where E_{m_S} is the energy of the spin sublevel $m_S = \pm 1/2, \pm 3/2$, T is the temperature, k_B is the Boltzmann constant, ρ is the mass density, and $\bar{v} = 5 v_l v_t / (2 v_t + 3 v_l)$

TABLE I: Mechanical parameters of 4H-SiC [31]

Mass density	$\rho = 3.2\,\mathrm{g/cm^3}$
Young modulus	$E = 4.7 \times 10^{12}\,\mathrm{dyn/cm^2}$
Poisson ratio	$\sigma = 0.14$
Velocity of longitudinal phonons	$v_l = 12.2 \times 10^5\,\mathrm{cm/s}$
Velocity of transverse phonons	$v_t = 8.0 \times 10^5\,\mathrm{cm/s}$

is the averaged velocity of longitudinal and transverse phonons. The spin transition rate $W^{(\mathrm{direct})}_{\pm 3/2,\mp 1/2}$ is given by the same equation (2), where $E_{\pm 1/2}$ should be replaced with $E_{\mp 1/2}$. The other spin transition rates vanish, $W^{(\mathrm{direct})}_{+3/2,-3/2} = W^{(\mathrm{direct})}_{+1/2,-1/2} = 0$. The presence of spin transitions with the spin projection change by ± 1 and ± 2 is the direct consequence of the interaction Hamiltonian (1) being quadratic in spin operators.

With increasing temperature, the Raman processes that involve absorption and emission of two thermal-energy phonons give the dominant contribution to the spin transitions [28]. The corresponding transition rates read

$$W^{(\mathrm{R})}_{\pm 3/2,\pm 1/2} = W^{(\mathrm{R})}_{\pm 3/2,\mp 1/2} = \frac{2\pi \Xi^4 k_B^5}{15\hbar^7 \rho^2 \bar{v}^{10}} T^5 , \qquad (3)$$

and the rates $W^{(\mathrm{R})}_{+3/2,-3/2}$ and $W^{(\mathrm{R})}_{+1/2,-1/2}$ are twice higher. The temperature dependence of the spin-lattice relaxation time T_1 of the V_{Si}(V2) spin qudit in 4H-SiC has been experimentally investigated in detail [29, 30]. It has been observed that $1/T_1$ increases linearly with temperature as $A_1 T$ up to 30 K and follows $A_5 T^5$ at high temperatures, in accord with Eqs. (2) and (3). Using the parameters of 4H-SiC (table I) together with the experimental value $A_5 = 1.1 \times 10^{-9}\,\mathrm{s^{-1}/K^5}$ [29], we estimate the deformation potential constant $\Xi \approx 2\,\mathrm{meV}$. It gives the direct transition rate $A_1 = 0.2 \times 10^{-2}\,\mathrm{s^{-1}/K}$ for the energy difference of $|E_{\pm 3/2} - E_{\pm 1/2}| = 500\,\mathrm{MHz}$ in Eq. (2), which is within the same order of magnitude with the experimental value $A_1 = 1.0 \times 10^{-2}\,\mathrm{s^{-1}/K}$ [29].

The small discrepancy in A_1 may be related to the parameter spread in the literature. Furthermore, the spin relaxation rates for the direct and Raman processes were obtained under the assumption of infinite isotropic medium. The recent *ab initio* calculations show that the spin-phonon interaction in SiC is anisotropic [27]. While these aspects may quantitatively modify our results, the conclusions drawn remain qualitatively unchanged. Importantly, the spin-phonon interaction is affected strongly by the structure design. In what follows we present theoretical results for spin centers coupled to quantized mechanical vibrations of a rectangular membrane.

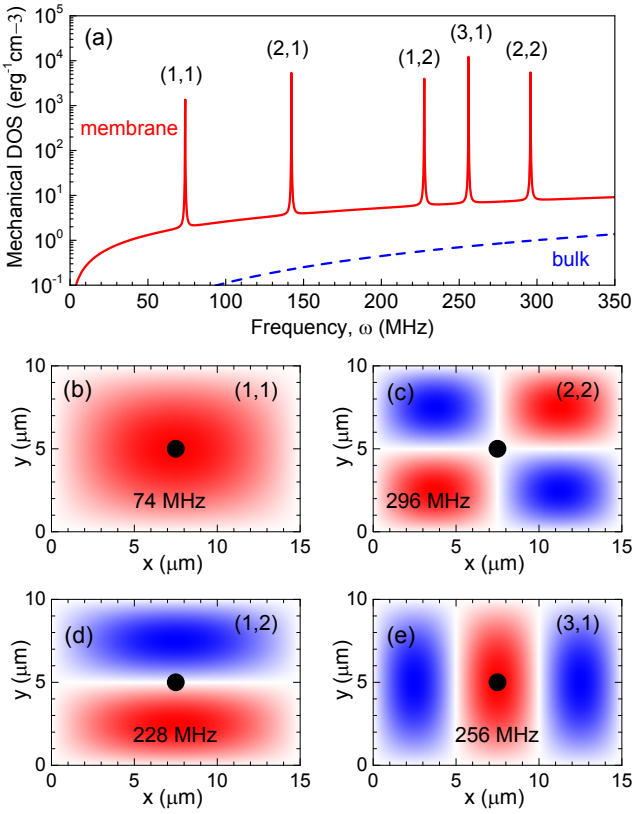

FIG. 1: Membrane eigenmodes. (a) Mechanical DOS in a $10\,\mu\mathrm{m} \times 15\,\mu\mathrm{m}$ SiC membrane with $Q = 10^4$ (solid line). The sharp peaks correspond to vibrational modes. For comparison, mechanical DOS in bulk SiC is shown by the dashed line. (b)–(e) Displacement distribution maps for various vibrational modes (labeled in each plot). Red and blue color corresponds to positive and negative displacement. The solid circle in the middle of the membrane indicates the position of the V_{Si} centers.

III. QUANTIZED MECHANICAL VIBRATIONS OF A MEMBRANE

To be specific, we consider a rectangular membrane with dimensions $L_x \times L_y = 10\,\mu\mathrm{m} \times 15\,\mu\mathrm{m}$ (Fig. 1) and a thickness $h = 1\,\mu\mathrm{m}$. We suppose that initially the membrane is not stressed and its ends are supported. Particularly, such a membrane can be fabricated on the 4H-SiC platform using epitaxial growth in combination with dopant-selective photoelectrochemical etch, as has previously been used for the fabrication of high-Q photonic crystals [32]. We assume that the mechanical quality factor of the membrane is $Q = 10^4$ [33, 34].

The system can support mechanical vibrations characterized by (i) in-plane and (ii) out-of-plane displacement. Both of them have only the in-plane component of the wave vector. The reason is that the out-of-plane wave vector component is quantized, which would result in frequencies $\sim \pi\bar{v}/h$, which are higher than the spin transition frequencies considered below. The in-plane

vibrational modes are similar to the acoustic waves in bulk material, with the same transverse sound velocity $v_t = \sqrt{E/[2\rho(1+\sigma)]}$ and different longitudinal sound velocity $v_l' = \sqrt{E/[\rho(1-\sigma^2)]}$ [35]. Here E is the Young modulus σ is the Poisson ratio.

The out-of-plane membrane displacement ζ is governed by the equation

$$h\rho\frac{\partial^2\zeta}{\partial t^2} + \mathcal{D}\Delta^2\zeta = 0\,, \tag{4}$$

where $\mathcal{D} = Eh^3/[12(1-\sigma^2)]$ and Δ is a two-dimensional Laplace operator. An appropriate boundary conditions, determined by how the membrane is attached to the environment should be imposed. For the sake of simplicity, we assume that the edges are supported. The eigenmodes of the system then read [35]

$$\zeta^{(j)}(x,y) = \sqrt{\frac{2\hbar}{\rho h\omega_j L_x L_y}}\sin\left(\frac{\pi n_x x}{L_x}\right)\sin\left(\frac{\pi m_y y}{L_y}\right), \tag{5}$$

and the corresponding eigenfrequencies are

$$\omega_j = \sqrt{\frac{\mathcal{D}}{h\rho}}\left[\left(\frac{n_x}{L_x}\right)^2 + \left(\frac{n_y}{L_y}\right)^2\right], \tag{6}$$

where $j = (n_x, n_y)$ with integer $n_x, n_y \geq 1$ enumerating the vibrational modes.

The mechanical density of states (DOS) for the parameters of table I is presented in Fig. 1(a). It is calculated as

$$\bar{D}(\omega) = \frac{\omega(v_l'^{-2} + v_t^{-2})}{2\pi h} + \frac{1}{\pi h L_x L_y}\sum_j \frac{\Gamma_j}{(\omega-\omega_j)^2 + \Gamma_j^2}\,, \tag{7}$$

where the first term stems from in-plane vibrations, while the second term represents the out-of plane modes. Γ_j is the decay rate of the vibrational mode j, which can be expressed via the mechanical quality factor Q as $\Gamma_j = \omega_j/(2Q)$. For comparison, we also show DOS of 3D phonons in the bulk material given by $\bar{D}(\omega) = \omega^2(v_l^{-3} + 2v_t^{-3})/(2\pi^2)$. The superior mechanical DOS of the membrane and the presence of mechanical resonances makes this system favorable for the study of spin-mechanical effects. The displacement for several membrane eigenmodes, $j = (1,1)$, $(2,2)$, $(1,2)$ and $(3,1)$ is illustrated in Figs. 1(b)-(e), respectively.

IV. RESULTS AND DISCUSSION

A. Low-temperature ODSMR magnetometry

The idea of the magnetometry is illustrated in Fig. 2(a). Upon application of the external magnetic field B_z along the c-axis, the V_{Si}(V2) spin states are split and shift linearly with B_z. Optical excitation results in the preferential population of the $m_S = \pm 1/2$ states [solid circles in Fig. 2(a)] [18]. After the excitation is switched off, the spin relaxation $\pm 1/2 \to \pm 3/2$ occurs. At low temperature, this relaxation is caused by the absorption or emission of single phonons, and typical relaxation time is on the order of 10 seconds [30]. However, in certain magnetic fields, when the splitting between some spin sublevels is equal to a membrane eigenfrequency [vertical arrows in Fig. 2(a)], the spin relaxation is accelerated due to the resonantly enhanced probability of phonon emission or absorption.

This effect can be described in terms of spin transitions induced by oscillating deformations $u_{\alpha\beta}^{(j)}$ [Eq. (1)], which are in turn caused by the periodical mechanical displacement of the membrane $\zeta^{(j)}$ [Eq. (5)]. In a thin membrane, the deformation is distributed linearly along the normal of the membrane and its maximal value

$$u_{\alpha\beta}^{(j)} = -\frac{h}{2}\frac{\partial^2\zeta^{(j)}}{\partial r_\alpha \partial r_\beta}\ (\alpha = x,y), \quad u_{zz}^{(j)} = \frac{h}{2}\frac{\sigma}{1-\sigma}\Delta\zeta^{(j)} \tag{8}$$

occurs at the membrane surface. It what follows, we assume that the spin centers are created close to the surface and in the center of the membrane [as shown schematically in Fig. 1(b-e)] unless explicitly mentioned. Technically, this can be realized using focused ion beam [36].

We now calculate the spin transition rates induced by the interaction with the membrane vibrations. The transitions with the spin projection change by $\Delta m_S = 1$ are governed by u_{xz} and u_{yz} strain components, that vanish for the mechanical membrane modes. The spin transition rate with $\Delta m_S = 2$ [vertical arrows in Fig. 2(a)], caused by the vibrations in mode j, is given by

$$W_{\pm 3/2,\mp 1/2}^{(j)} = \frac{3}{2}\frac{\Xi^2|u_{xx}^{(j)} \pm 2\mathrm{i}u_{xy}^{(j)} - u_{yy}^{(j)}|^2\Gamma_j N_j}{(|E_{\pm 3/2} - E_{\mp 1/2}| - \hbar\omega_j)^2 + \hbar^2\Gamma_j^2}\,, \tag{9}$$

where N_j is the number of phonons in the mode, which is given by $\overline{N}_j = k_B T/(\hbar\omega_j)$ in the thermal equilibrium.

Figure 2(b) shows the spin relaxation times $(\sum_j W_{+3/2,-1/2}^{(j)})^{-1}$ (blue) and $(\sum_j W_{-3/2,+1/2}^{(j)})^{-1}$ (red), calculated as a function of the magnetic field using Eq. (9). At certain magnetic fields, the spin relaxation time drops down by two orders of magnitude. This occurs when the spin splitting between the $m_S = +3/2$ and $m_S = -1/2$ states or between the $m_S = -3/2$ and $m_S = +1/2$ states is equal to the eigenfrequency ω_j of mode $j = (n_x, n_y)$ with odd n_x and n_y. Indeed, according to Eq. (5), only such "bright" modes have non-zero deformation in the middle of the membrane and hence interact with spin centers [Figs. 1(b)-(e)]. Furthermore, our calculations predict an increase of the relaxation time by two orders of magnitude ($> 1000\,\mathrm{s}$) at $B_z = 1.25\,\mathrm{mT}$ due to the second ground state level anticrossing (GSLAC-2) [37].

Figure 2(c) presents an all-optical protocol to detect the spin-mechanical modes. The system is excited by a sequence of short optical pulses, leading to the preferential population of the $m_S = 1/2$. The population difference diminishes between these pulses due to the spin relaxation processes of Eq. (9). The photoluminescence (PL) of V_{Si} is spin-dependent, i.e., contains a contribution proportional to the population difference between the $m_S = \pm 1/2$ and $m_S = \pm 3/2$ states [18]. Therefore, it can be deduced from $\Delta PL_0 = PL_r - PL_0$, where PL_r is the reference PL recorded immediately after the pump laser is switched on and PL_0 is recorded at the end of the laser pulse, when the spin pumping takes place. The next measurement PL_τ is performed with variable delay τ and, consequently, $\Delta PL_\tau = PL_r - PL_\tau$ depends on the spin relaxation time.

Figure 2(d) shows $\Delta PL_\tau/\Delta PL_0$ as a function of the magnetic field calculated using the spin relaxation time of Fig. 2(b) for two values of delay τ. As expected, pronounced dips for $\tau = 3\,$s correspond to "bright" mechanical modes of the membrane. The full width half maximum (FWHM) of these deeps depends on τ, becoming narrow for shorter delay times. The grey area in Fig. 2(d) zooms in on the optically detected spin-mechanical resonance (ODSMR) at $70\,\mu$T. For $\tau = 1\,$ms, we obtain the FWHM $\Lambda_\omega = 0.3\,\mu$T. For comparison, a typical FWHM of the optically detected magnetic resonance (ODMR) lines associated with the V_{Si} centers in SiC is about $100\,\mu$T [24]. In case of ODSMR the magnetic field sensitivity depends on the mechanical quality factor Q and spin relaxation time T_1, while in case of ODMR it is determined by the spin coherence time T_2. For $T_1 \gg T_2$ and high $Q \gg \omega_j T_2$, the ODSMR-based protocol provides higher sensitivity. For brevity, we assume 100% efficiency ($\alpha = 1$) of the spin read-out at low temperature [38, 39], 100% spin polarization ($\Delta f = 1$) [30] and the photon count rate from a single V_{Si} defect $R = 4 \times 10^4\,$Hz [40, 41]. It yields DC magnetic field sensitivity $\delta B_{\min} = \Lambda_\omega/\sqrt{RN_d} \sim 1/\sqrt{N_d}\ \mathrm{nT}\cdot\mathrm{Hz}^{-1/2}$, where N_d is the number of the V_{Si} defects. We note that for dense spin ensembles, inhomogeneous broadening can eliminate the advantage of the ODSMR protocol.

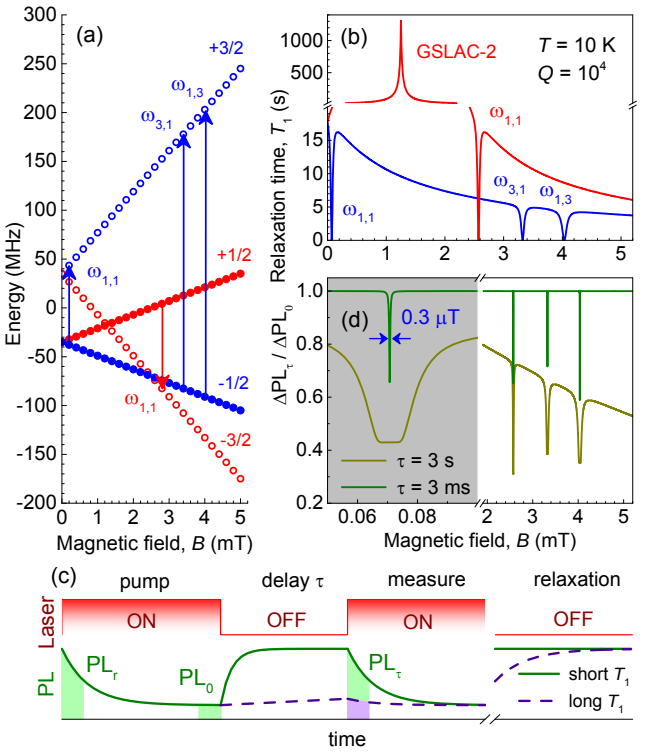

FIG. 2: Spin-mechanical magnetometry. (a) The GS spin sublevels of the V_{Si}(V2) qudit in the external magnetic field B_z. The solid (open) circles represent the preferentially populated (depleted) states under optical pumping. The vertical arrows indicate available spin transitions frequencies ω_j due to interaction with membrane modes $j = (n_x, n_y)$ in case when the V_{Si} qudit center is placed in the middle of the membrane, as shown in Fig. 1(b)–(e). (b) Spin relaxation time T_1 between the $-1/2 \to +3/2$ (red) and $+1/2 \to -3/2$ (blue) spin sublevels. The deeps correspond to the membrane modes. The peak at 1.25 mT is due to the ground state level anticrossing. (c) An all-optical protocol to probe spin-mechanical modes. The solid and dashed line correspond to the PL variation in case of short (resonant) and long (non-resonant) spin relaxation. (d) Relative PL difference with $\Delta PL_{0,\tau} = PL_r - PL_{0,\tau}$ as a function of B_z for different deleays τ. The grey area highlights the optically detected spin-mechanical resonance at $70\,\mu$T with calculated FWHM of $0.3\,\mu$T for $\tau = 1\,$ms.

B. Room-temperature nonlinear effects in the strong pumping regime

In the aforementioned discussion, we assume that the number of quanta in the vibrational modes corresponds to the environment temperature. However, when a single mechanical mode interacts with many spin centers that are driven from thermal equilibrium by optical pump, the effective temperature of the mode can deviate from that of the environment [13]. In case of spin-3/2 centers, this process can be qualitatively understood from Fig. 2(a). At a magnetic field of 2.57241 mT, corresponding to ODSMR with the $\omega_{1,1}$ mode, the spin relaxation leads to phonon emission. As a result, the number of phonon increases, which can be described as an increase of the effective temperature of the $\omega_{1,1}$ mode. On the contrary, at a magnetic field of 0.07072 mT, also corresponding to ODSMR with the $\omega_{1,1}$ mode, the spin relaxation leads to phonon absorption. As a result, the effective temperature of the $\omega_{1,1}$ mode decreases.

To describe theses heating and cooling processes under ODSMR, we use the rate equation approach. The dynamics of the spin level occupancies f_{m_S} ($m_S = +3/2, +1/2, -1/2, -3/2$) in an ensemble of spin centers under optical pumping is given by the following equation

set

$$\frac{df_s}{dt} = \sum_{m'_S} \left(W^{(\mathrm{R})}_{m_S,m'_S} + \sum_j W^{(j)}_{m_S,m'_S} \right) (f_{m'_S} - f_{m_S}) + IP_{m_S,m'_S} f_{m'_S} \,. \quad (10)$$

Here, I is the pump intensity, P describes pump-induced transitions, $W^{(j)}$ is given by Eq. (9). Since the phonon, involved in the Raman process of spin relaxation, have high energy and do not feel the confinement, we use the bulk expression of Eq. (3) for $W^{(\mathrm{R})}$. Optical pumping leads to preferable occupancy of either the $\pm 3/2$ or $\pm 1/2$ spin states, depending on the type of the spin center. In order to describe this, we assume that the PL cycle rate when the spin center goes from the $\pm 3/2$ state to the $\pm 1/2$ state is given by ηI, while the PL cycle rate when spin center goes from the $\pm 1/2$ state to the $\pm 3/2$ state is $\eta' I$. The corresponding optical pump matrix read

$$P = \begin{pmatrix} -\eta & \frac{\eta'}{2} & \frac{\eta'}{2} & 0 \\ \frac{\eta}{2} & -\eta' & 0 & \frac{\eta}{2} \\ \frac{\eta}{2} & 0 & -\eta' & \frac{\eta}{2} \\ 0 & \frac{\eta'}{2} & \frac{\eta'}{2} & -\eta \end{pmatrix} . \quad (11)$$

The maximal spin polarization degree achieved at high intensities $I \to \infty$ is $\Delta f = f_{+3/2} + f_{-3/2} - f_{+1/2} - f_{-1/2} = (\eta - \eta')/(\eta + \eta')$. The experimentally obtained value $f_{+1/2} - f_{+3/2} \approx f_{-1/2} - f_{-3/2} \approx 0.03$ for the V_{Si} centers at room temperature [30] gives $\eta/\eta' \approx 1.1$.

The transition rates $W^{(j)}$ are proportional to the numbers of the vibrational quanta N_j. In order to determine them, we use the corresponding rate equations,

$$\frac{dN_j}{dt} = \sum_{m'_S, m_S} \theta(E_{m'_S} - E_{m_S}) N_d W^{(j)}_{m_S,m'_S} (f_{m'_S} - f_{m_S}) - (N_j - \overline{N}_j) \frac{\omega_j}{Q}, \quad (12)$$

where N_d is the number of spin centers that interact with mode ω_j, and θ is the Heaviside function. The simultaneous solution of coupled non-linear equations (10)-(12) allows us to calculate the steady-state spin level occupancies f_{m_S} and vibration quanta numbers N_j. The PL intensity change is then given by

$$\frac{\Delta \mathrm{PL}}{\mathrm{PL}} = \alpha (f_{+3/2} + f_{-3/2} - f_{+1/2} - f_{-1/2}) = \alpha \Delta f \quad (13)$$

where the dimensionless parameter $\alpha \approx 0.1$ quantifies the efficiency of optical spin read-out [30, 42].

The results of these calculations for room temperature and with mechanical quality factor $Q = 6 \times 10^4$ are presented in Fig. 3(a). In case of a single V_{Si} center ($N_d = 1$), our model predicts sharp peaks in the PL intensity as a function of the magnetic field. The heights of these peaks are equal for the same mechanical mode. Particularly, the dashed line in Fig. 3(a) shows the ODSMR lines for the lowest mode (1,1).

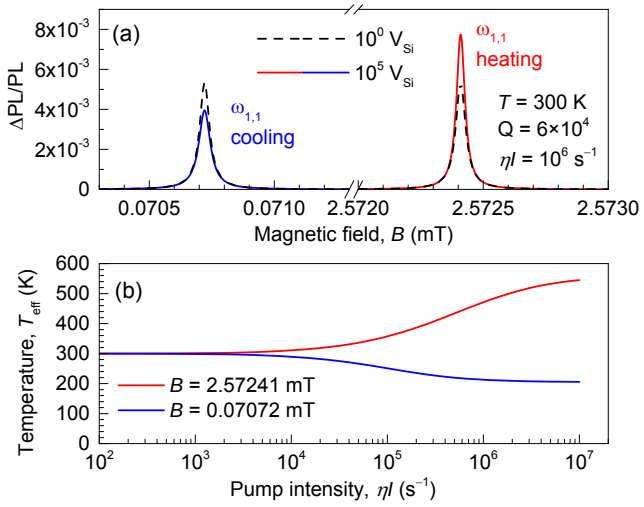

FIG. 3: Non-linear effects in the strong pumping regime. (a) Relative change ΔPL/PL as a function of the magnetic field applied along the c-axis for pump intensity $\eta I = 10^6\,\mathrm{s}^{-1}$. The peaks at 0.07072 mT and 2.57241 mT correspond to ODSMR with the vibrational mode (1,1). The dashed and solid lines are the calculation for a single V_{Si} and 10^5 V_{Si} centers, respectively. The difference in the peak amplitude indicates heating and cooling of the vibrational mode. (b) Effective temperature of the vibrational mode (1,1) as a function of pump intensity for 10^5 V_{Si} centers at two magnetic fields corresponding to ODSMR.

For a great number of spin centers ($N_d = 10^5$) in the middle of the membrane, the nonlinear effects become visible, as shown by the solid lines in Fig. 3(a). Due to lower steady-state number of vibration quanta N_j at 0.07072 mT (phonon absorption) and higher at 2.57241 mT (phonon emission), the ODSMR lines have different heights.

The difference of N_j from its equilibrium value $\overline{N}_j$ can be interpreted as optically induced mode heating or cooling, with the effective temperature of the mode $T^{(j)}_{\mathrm{eff}} = N_j \hbar \omega_j / k_B$. The effective temperature depends on the pump intensity ηI as shown in Fig. 3(b). The heating/cooling process can be quite efficient at high pump intensities. Remarkably, our model predicts optical cooling of the lowest vibrational mode (1,1) from room temperature to approximately 200 K for $\eta I > 3 \times 10^6\, s^{-1}$.

To estimate the laser powers required for the observation the aforementioned nonlinear effects, we first determine the characteristic pump intensity ηI_0, when the spin polarization occurs. To do this, we consider Eq. (10) with $W^{(j)}_{m_S,m'_S} = 0$ (spin relaxation is dominated by the Raman process as in the bulk). The steady-state solution yields $\eta I_0 \sim W^{(\mathrm{R})}_{\pm 3/2,\pm 1/2} \sim 3 \times 10^3\, s^{-1}$. This value is related to the characteristic laser power of about 0.1 mW μm^{-2} [30]. We assume that the V_{Si} ensemble with an area of 10 μm^2 is created in the middle of the membrane. With 10^5 V_{Si} centers, this corresponds to the density of 10^{16} cm^{-3}. Putting all together, we conclude that the pump inten-

sity ηI of $3\times10^6\,s^{-1}$, as required to observe pronounced cooling effects of the membrane modes, can be achieved with a laser power of about 1 W. Taking the absorption cross section of the $V_{\rm Si}$ centers into account [30, 41], only about 5% of 1 W are absorbed in the $h = 1\,\mu m$ thick membrane, minimizing heating effect due to the direct laser absorption.

C. Mass detection with ODSMR

Suppose a particle with small mass m gets attached to the membrane at coordinates (x, y). As a consequence, the resonant frequencies of the mechanical modes are shifted

$$\Delta\omega_{n_x,n_y} = -\frac{4m\omega_{n_x,n_y}}{M}\sin^2\frac{n_x\pi x}{L_x}\sin^2\frac{n_y\pi y}{L_y}\,, \qquad (14)$$

where $M = \rho h L_x L_y$ is the membrane mass. Figure 4(a) shows an example for the ODSMR modes for $Q = 10^4$, $m/M = 10^{-4}$ and different mass positions A and B. The position A corresponds to the membrane center ($x = 7.5\,\mu$m, $y = 7.5\,\mu$m) and position B corresponds to the shift along the x axis ($x = 11.25\,\mu$m, $y = 7.5\,\mu$m), as shown schematically in the inset of Fig. 4(b).

Using the ODSMR shifts corresponding to different modes, one can determine both the position of the attached particle and its mass. In particular, it follows from Eq. (14)

$$\frac{\delta\omega_{n_x,1}}{\delta\omega_{1,1}} = \frac{\sin^2(n_x\pi x/L_x)}{\sin^2(\pi x/L_x)}\,, \qquad (15)$$

where $\delta\omega_{n_x,n_y} = \Delta\omega_{n_x,n_y}/\omega_{n_x,n_y}$. The x-coordinate can be unambiguously found from analysing several odd $(n_x, 1)$ modes [Fig.4(b)] and the y-coordinate can be found in the similar way analyzing odd $(1, n_y)$ modes. The attached particle mass is given by

$$m = \frac{4M\delta\omega_{1,1}}{(3-\sqrt{\delta\omega_{1,3}/\delta\omega_{1,1}})(3-\sqrt{\delta\omega_{3,1}/\delta\omega_{1,1}})}\,. \qquad (16)$$

The mass sensitivity is determined by the membrane mass M and the measurement accuracy of the relative ODSMR shift $\delta\omega_{1,1}$. The latter depends on the mechanical quality factor Q and the accuracy to measure ΔPL/PL from Eq. (13). We estimate the minimum detectable ODSMR shift as a product

$$\delta\omega_{\rm min} = \frac{1}{Q_S}\frac{1}{\alpha\Delta f}\frac{1}{\sqrt{RN_d}}\,. \qquad (17)$$

Here, $Q_S = \omega_j/\Lambda_\omega$ is an effective ODSMR Q-factor. We obtain from Fig. 4(a) $Q_S = 10^2$. Note, for the protocol of Fig. 2(c) Q_S tends to the mechanical quality factor Q. The readout efficiency α and spin polarization Δf yield $\alpha\Delta f = 3\times10^{-3}$ at room temperature and $\alpha\Delta f \sim 1$ at low temperature [30, 38, 39]. The photon count rate

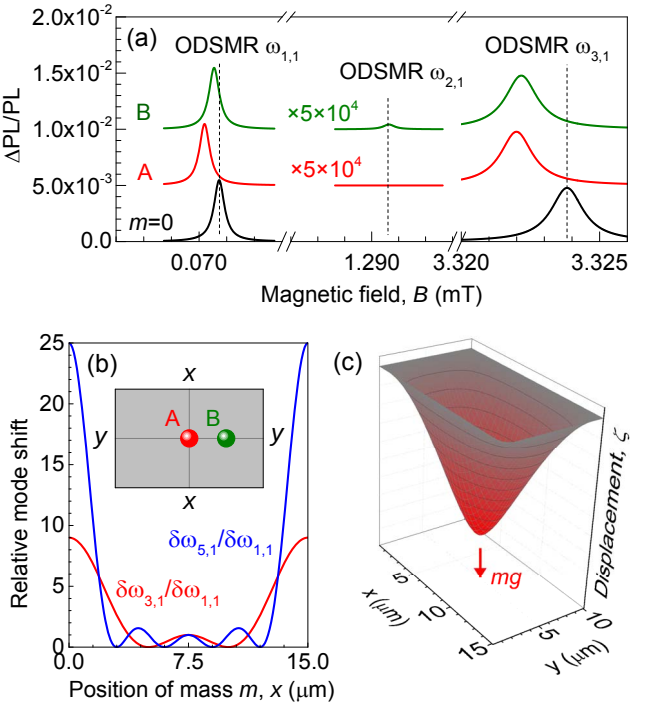

FIG. 4: Mass effect on the ODSMR modes. (a) Relative change ΔPL/PL as a function of the magnetic field for positions A and B of the probe mass. The calculations are performed for $m/M = 0$ (the lowest curves) and $m/M = 10^{-4}$ with mechanical Q-factor 10^4. The peaks at 0.0707 mT, 1.2906 mT and 3.3238 mT correspond to ODSMR with vibrational modes (1,1), (2,1) and (3,1), respectively. (b) Relative difference of the mass-induced shift of the ODSMR lines $\delta\omega_{n_x,1}/\delta\omega_{1,1}$ (with $n_x = 3, 5$) as a function of the position of the probe mass m. Inset indicates positions A and B on the membrane. (c) Displacement of the membrane $\zeta(x, y)$ due to inertia force mg, when a particle of mass m is placed in the center.

from a single $V_{\rm Si}$ defect is $R = 4\times10^4$ Hz [40, 41]. We then estimate $\delta\omega_{\rm min} \sim 10^{-2}/\sqrt{N_d}\,{\rm Hz}^{-1/2}$ at room temperature and $\delta\omega_{\rm min} \sim 10^{-6}/\sqrt{N_d}\,{\rm Hz}^{-1/2}$ for the optimized protocol at cryogenic temperature. With the membrane mass $M = 0.5$ ng for the given dimensions, wir obtain the mass sensitivity $\delta m_{\rm min} \sim 10/\sqrt{N_d}$ pg $\cdot$ Hz$^{-1/2}$ and $\delta m_{\rm min} \sim 1/\sqrt{N_d}$ fg $\cdot$ Hz$^{-1/2}$, respectively. According to these estimations, ultrahigh zg sensitivity can be achieved by increasing the mechanical (ODSMR) quality factor Q (Q_S) and reducing the membrane mass M. This should allow mass detection of individual macromolecules [16].

We now discuss another effect, when a particle is placed not in the geometrical center of the membrane. In this case the mixing of the vibrational modes occurs. As a result, the dark modes that in the unperturbed case are not detectable due to their symmetry, e.g., mode $(2, 1)$, get an admixture of bright modes and appear in the ODSMR spectra. The admixture amplitude of the

mode $j' = (n'_x, n'_y)$ to mode $j = (n_x, n_y)$ reads

$$\alpha_{jj'} = \frac{4m}{M} \frac{\omega_j^2}{\omega_{j'}^2 - \omega_j^2} \sin\frac{n_x \pi x}{L_x} \sin\frac{n_y \pi y}{L_y} \sin\frac{n'_x \pi x}{L_x} \sin\frac{n'_y \pi y}{L_y} . \tag{18}$$

Then, the relaxation rate in the vicinity of the dark mode frequency ω_j is given by

$$W^{(j)}_{\pm 3/2, \mp 1/2} = \frac{3}{2} \frac{\Xi^2 |\sum_{j'} \alpha_{jj'} (u^{(j')}_{xx} \pm 2\mathrm{i} u^{(j')}_{xy} - u^{(j')}_{yy})|^2 \Gamma_j N_j}{(|E_{\pm 3/2} - E_{\mp 1/2}| - \hbar\omega_j)^2 + \hbar^2 \Gamma_j^2} , \tag{19}$$

Figure 4(a) compares the calculated amplitude of the mode $(2, 1)$ for $m/M = 10^{-4}$ when the particle is placed in center of the membrane and and shifted along the x axis, i.e., positions A and B respectively. This effect can be also used to determine the position of the particle, however it is less sensitive compared to the method discussed above.

D. ODSMR accelerometry

We consider now a static deflection of the membrane caused by some external force.The material deformation around the spin center modifies its fine structure, which can be described by the perturbation of the effective spin Hamiltonian (1)

$$V = \delta D (S_z^2 - \tfrac{5}{4}) + \tfrac{1}{2}(\delta E\, S_+^2 + \delta E^* S_-^2) , \tag{20}$$

where $S_\pm = S_x \pm S_y$, $\delta D = \Xi(u_{zz} - \frac{1}{2}u_{xx} - \frac{1}{2}u_{yy})$ describes variation of the zero-field splitting, and $\delta E = \Xi(\frac{1}{2}u_{xx} - \frac{1}{2}u_{yy} - \mathrm{i}u_{xy})$ mixes the $m_S = \pm 1/2$ and $m_S = \mp 3/2$ spin states. Using the expression for the deformation components of Eq. (8), we obtain

$$\delta D = \Xi \frac{h}{4} \frac{1+\sigma}{1-\sigma} \Delta\zeta . \tag{21}$$

The value of δD, directly available as a shift of the ODSMR line. Measurement of this shift with spatial resolution can be used to map the membrane bending $\Delta\zeta(x, y)$.

A possible application of the proposed bending measurement is a detection of the acceleration g. To this end, a particle of a large known mass m is placed in the center of the membrane. The inertia force mg produces a load in the membrane center. Figure 4(c) presents membrane deflection $\zeta(x, y)$ as a function of the x and y coordinates induced by such a load. The maximum membrane bending is achieved in the membrane center and reads $\Delta\zeta_0 = Cmg/\mathcal{D}$, where C is a constant of the order of unity, determined by the membrane and particle dimensions. For the particle size $d \ll L_x, L_y$ and $m \gg M$, it is given by $C \approx (1/2\pi)\ln(d/L_x)$. Then, by measuring the zero-field splitting variation δD one calculates the inertia force from

$$\frac{mg}{\delta D} = \frac{Eh^2}{3C(1+\sigma)^2 \Xi} . \tag{22}$$

For the parameters from table I, the deformation potential constant $\Xi \approx 2\,\mathrm{meV}$ and the membrane thickness $h = 1\,\mu\mathrm{m}$, we estimate using Eq. (22) $mg/\delta D \sim 0.1\,\mathrm{g \cdot cm \cdot s^{-2}/MHz}$.

The minimum detectable zero-field splitting variation can be estimated using Eq. (17) as $\delta D_{\min} = D\delta\omega_{\min}$. We assume that a gold ($19.3\,\mathrm{g/cm^3}$) sphere with a diameter of $1\,\mu\mathrm{m}$ is attached to the center of the membrane, which has a mass of 80 pg. Combining Eq. (22) and Eq. (17), we estimate the room-temperature acceleration sensitivity $g_{\min} \sim 5 \times 10^8/\sqrt{N_d}\ \mathrm{cm \cdot s^{-2} \cdot Hz^{-1/2}}$. In fact, this sensitivity is miserable because of membrane dimensions are not optimal for the acceleration measurement. The sensitivity can be dramatically improved by using very thing membranes. For instance, if the thickness of the membrane is $h = 10\,\mathrm{nm}$ instead of $h = 1\,\mu\mathrm{m}$, the sensitivity is improved by 4 orders of magnitude. Attaching a heavier particle to the membrane center is another way to improve the acceleration sensitivity. For instance, a gold sphere with a diameter of $10\,\mu\mathrm{m}$ should give further improvement by 3 orders of magnitude. Thus, the room temperature sensitivity better than $g_{\min} \sim 50/\sqrt{N_d}\ \mathrm{cm \cdot s^{-2} \cdot Hz^{-1/2}}$ is feasible though technologically challenging. Further improvement is possible using membranes with larger lateral dimensions, however the mechanical resonance frequencies shift to the sub-MHz range.

V. CONCLUSIONS

We have considered theoretically the optically detected spin-mechanical resonance associated with half-integer spin centers in SiC membranes. It is caused by the spin-phonon coupling and occurs when the conditions for the spin resonance and mechanical resonance are simultaneously fulfilled. Due to the optical spin pumping mechanism and spin-dependent recombination, ODSMR is detected as a change in the PL intensity. Based on these properties, we have proposed all-optical sensing protocols, where the sensitivity is determined by the mechanical quality factor. We have discussed the realistic conditions, under which the femtotesla-scale magnetic sensing and zeptogram-scale mass sensing can be achieved. By placing a micron-size particle at the center of the membrane, the ODSMR can be used as an accelerometer. In addition, we have considered the application of strong optical pumping of a dense spin ensemble in a membrane for cooling of the mechanical modes from room temperature to below 200 K. Our findings suggest that hybride SiC spin-mechanical systems are a promising platform for quantum sensing applications.

[1] M. Aspelmeyer, T. J. Kippenberg, and F. Marquardt, Reviews of Modern Physics **86**, 1391 (2014).

[2] A. G. Krause, M. Winger, T. D. Blasius, Q. Lin, and O. Painter, Nature Photonics **6**, 768 (2012).

[3] J. Bochmann, A. Vainsencher, D. D. Awschalom, and A. N. Cleland, Nature Physics **9**, 712 (2013).

[4] J. R. Maze, A. Gali, E. Togan, Y. Chu, A. Trifonov, E. Kaxiras, and M. D. Lukin, New Journal of Physics **13**, 025025 (2011).

[5] M. W. Doherty, N. B. Manson, P. Delaney, and L. C. L. Hollenberg, New Journal of Physics **13**, 025019 (2011).

[6] P. Udvarhelyi, V. O. Shkolnikov, A. Gali, G. Burkard, and A. Pályi, arXiv p. 1712.02684 (2017).

[7] O. Arcizet, V. Jacques, A. Siria, P. Poncharal, P. Vincent, and S. Seidelin, Nature Physics **7**, 879 (2011).

[8] S. Kolkowitz, A. C. Bleszynski Jayich, Q. P. Unterreithmeier, S. D. Bennett, P. Rabl, J. G. E. Harris, and M. D. Lukin, Science **335**, 1603 (2012).

[9] P. Ovartchaiyapong, K. W. Lee, B. A. Myers, and A. C. B. Jayich, Nature Communications **5** (2014).

[10] E. R. MacQuarrie, T. A. Gosavi, A. M. Moehle, N. R. Jungwirth, S. A. Bhave, and G. D. Fuchs, Optica **2**, 233 (2015).

[11] A. Barfuss, J. Teissier, E. Neu, A. Nunnenkamp, and P. Maletinsky, Nature Physics **11**, 820 (2015).

[12] D. A. Golter, T. Oo, M. Amezcua, K. A. Stewart, and H. Wang, Physical Review Letters **116**, 143602 (2016).

[13] E. R. MacQuarrie, M. Otten, S. K. Gray, and G. D. Fuchs, Nature Communications **8**, 14358 (2017).

[14] M. S. J. Barson, P. Peddibhotla, P. Ovartchaiyapong, K. Ganesan, R. L. Taylor, M. Gebert, Z. Mielens, B. Koslowski, D. A. Simpson, L. P. McGuinness, et al., Nano Letters **17**, 1496 (2017).

[15] Y. T. Yang, K. L. Ekinci, X. M. H. Huang, L. M. Schiavone, M. L. Roukes, C. A. Zorman, and M. Mehregany, Applied Physics Letters **78**, 162 (2001).

[16] Y. T. Yang, C. Callegari, X. L. Feng, K. L. Ekinci, and M. L. Roukes, Nano Letters **6**, 583 (2006).

[17] M. Li, H. X. Tang, and M. L. Roukes, Nature Nanotechnology **2**, 114 (2007).

[18] D. Riedel, F. Fuchs, H. Kraus, S. Väth, A. Sperlich, V. Dyakonov, A. Soltamova, P. Baranov, V. Ilyin, and G. V. Astakhov, Physical Review Letters **109**, 226402 (2012).

[19] A. L. Falk, B. B. Buckley, G. Calusine, W. F. Koehl, V. V. Dobrovitski, A. Politi, C. A. Zorman, P. X. L. Feng, and D. D. Awschalom, Nature Communications **4**, 1819 (2013).

[20] A. L. Falk, P. V. Klimov, B. B. Buckley, V. Ivády, I. A. Abrikosov, G. Calusine, W. F. Koehl, A. Gali, and D. D. Awschalom, Physical Review Letters **112**, 187601 (2014).

[21] S. J. Whiteley, G. Wolfowicz, C. P. Anderson, A. Bourassa, H. Ma, M. Ye, G. Koolstra, K. J. Satzinger, M. V. Holt, F. J. Heremans, et al., arXiv p. 1804.10996 (2018).

[22] V. A. Soltamov, C. Kasper, A. V. Poshakinskiy, A. N. Anisimov, E. N. Mokhov, A. Sperlich, S. A. Tarasenko, P. G. Baranov, G. V. Astakhov, and V. Dyakonov, arXiv p. 1807.10383 (2018).

[23] E. Sörman, N. Son, W. Chen, O. Kordina, C. Hallin, and E. Janzén, Physical Review B **61**, 2613 (2000).

[24] H. Kraus, V. A. Soltamov, D. Riedel, S. Väth, F. Fuchs, A. Sperlich, P. G. Baranov, V. Dyakonov, and G. V. Astakhov, Nature Physics **10**, 157 (2014).

[25] H. Kraus, V. A. Soltamov, F. Fuchs, D. Simin, A. Sperlich, P. G. Baranov, G. V. Astakhov, and V. Dyakonov, Scientific Reports **4**, 5303 (2014).

[26] P. Udvarhelyi, V. O. Shkolnikov, A. Gali, G. Burkard, and A. Pályi, Physical Review B **98**, 075201 (2018).

[27] P. Udvarhelyi and A. Gali, Physical Review Applied **10**, 054010 (2018).

[28] A. Abragam and B. Bleaney, *Electron Paramagnetic Resonance of Transition Ions* (OUP Oxford, 2012).

[29] D. Simin, H. Kraus, A. Sperlich, T. Ohshima, G. V. Astakhov, and V. Dyakonov, Physical Review B **95**, 161201(R) (2017).

[30] M. Fischer, A. Sperlich, H. Kraus, T. Ohshima, G. V. Astakhov, and V. Dyakonov, Physical Review Applied **9**, 2126 (2018).

[31] O. Madelung, U. Rössler, and M. Schulz, eds., *Landolt-Börnstein. Group IV Elements, IV-IV and III-V Compounds* (Springer Berlin Heidelberg, 2001).

[32] D. O. Bracher and E. L. Hu, Nano Letters **15**, 6202 (2015).

[33] A. C. Barnes, R. C. Roberts, N. C. Tien, C. A. Zorman, and P. X. L. Feng, in *TRANSDUCERS 2011 - 2011 16th International Solid-State Sensors, Actuators and Microsystems Conference* (IEEE, 2011), pp. 2614–2617.

[34] L. G. Villanueva and S. Schmid, Physical Review Letters **113**, 227201 (2014).

[35] L. Landau, E. Lifshitz, and J. Sykes, *Theory of Elasticity* (Pergamon Press, 1989).

[36] H. Kraus, D. Simin, C. Kasper, Y. Suda, S. Kawabata, W. Kada, T. Honda, Y. Hijikata, T. Ohshima, V. Dyakonov, et al., Nano Letters **17**, 2865 (2017).

[37] D. Simin, V. A. Soltamov, A. V. Poshakinskiy, A. N. Anisimov, R. A. Babunts, D. O. Tolmachev, E. N. Mokhov, M. Trupke, S. A. Tarasenko, A. Sperlich, et al., Physical Review X **6**, 031014 (2016).

[38] P. G. Baranov, A. P. Bundakova, A. A. Soltamova, S. B. Orlinskii, I. V. Borovykh, R. Zondervan, R. Verberk, and J. Schmidt, Physical Review B **83**, 125203 (2011).

[39] R. Nagy, M. Widmann, M. Niethammer, D. B. R. Dasari, I. Gerhardt, Ö. O. Soykal, M. Radulaski, T. Ohshima, J. Vučković, N. T. Son, et al., Physical Review Applied **9**, 034022 (2018).

[40] M. Widmann, S.-Y. Lee, T. Rendler, N. T. Son, H. Fedder, S. Paik, L.-P. Yang, N. Zhao, S. Yang, I. Booker, et al., Nature Materials **14**, 164 (2015).

[41] F. Fuchs, B. Stender, M. Trupke, D. Simin, J. Pflaum, V. Dyakonov, and G. V. Astakhov, Nature Communications **6**, 7578 (2015).

[42] S. A. Tarasenko, A. V. Poshakinskiy, D. Simin, V. A. Soltamov, E. N. Mokhov, P. G. Baranov, V. Dyakonov, and G. V. Astakhov, physica status solidi (b) **255**, 1700258 (2018).